Chapter 6

Electrochemical sensing of dopamine and epinephrine in presence of excess ascorbic acid and uric acid using immobilized silver nanoparticles on self-assembled penicillamine modified gold electrode

6.1. Introduction

Dopamine (DA) and epinephrine (EP) are two important catecholamine neurotransmitters that communicate information throughout our brain and body. The brain uses these neurotransmitters to stimulate the heart for beating, lungs for breathing and stomach to digesting food.[1] Low levels or complete depletion of DA and EP in the central nervous system is implicated as a major cause of several neurological disorders like Parkinson's disease, Schizophrenia, Huntington's disease, as well as drug addiction and HIV.[2] Medically DA and EP are very common emergency health care medicine and have been used in hypertension, bronchial asthma, cardiac surgery, myocardial infection etc.[3] Thus it is necessary to develop quantitative methods for their sensitive and selective determination in a simultaneous way. Different methods are used to determine DA and EP simultaneously, including high performance liquid chromatography-mass spectroscopy,[4] capillary electrophoresis,[5] chemiluminescence,[6] flow injection analysis,[7] spectrophotometry [8] and electrochemical methods.[9] Due to simple procedures, high sensitivity, reproducibility, economic and ease of miniaturization electrochemical sensor were explored to determine DA and EP. Dopamine and epinephrine are often coexisting with ascorbic acid (AA) and uric acid (UA) in biological sample. In the electroanalytical methods at most solid electrodes, they can all be oxidized at similar potential resulting in an overlapping voltammetric response. Therefore, the simultaneous electrochemical detection of DA and EP in the presence of AA and UA is a real challenge in the field of pathological and drug development research. For their simultaneously detection many different strategies have been employed for the modification of electrode surface but only few electrochemical sensor has been exploited which can able to detect simultaneously DA, EP, AA and UA.[10] Among different modification process self-assembled monolayer (SAMs) of organosulphur compounds on metal surfaces comprise a wide range of potential applications due to their versatility in modifying surfaces in a controllable manner. It has been shown that organothiol molecules adsorb at gold via S-Au bond formation using oxidative addition and reductive elimination process.[11] Penicillamine, $(CH_3)_2C(SH)CH(NH_2)(COOH)$, can form highly stable self-assembled gold electrode

and used for the study of electrochemical behavior of DA and EP in an individual basis.[12, 13] The main drawback of such modified electrode is that they cannot detect DA and EP simultaneously because they oxidized at similar potential at Penicillamine-Au electrode. To overcome such limitation of penicillamine modified electrode, we introduce silver nanoparticles over penicillamine self-assembled gold electrode. Among different metal nanoparticles, silver nanoparticles are of special interest due to their catalytic properties.[14] Traditionally, AgNPs have been used as catalyst in various reactions. Beside this silver exhibits the highest electrical conductivity among all metals.[15] In the present communication we first time reported that AgNPs-penicillamine-Au electrode can detect DA and EP simultaneous in the presence of high concentration of AA and UA at neutral pH. A well separated oxidation peaks for DA, EP, AA and UA was observed at the AgNPs-penicillamine-Au electrode in phosphate buffer solution (pH 7.0). Diffusion coefficient, electron transfer coefficient and the catalytic reaction rate were also examined for DA and EP. The proposed modified gold electrode has been applied to the simultaneous voltammetric measurement of DA, EP and AA, UA in human blood sample with satisfactory results.

6.2. Experimental

6.2.1. Synthesis of silver nanoparticles

In an ethanolic solution of 0.001 M silver nitrate and 0.5 % PVP, 0.1 M ascorbic acid was added drop wise and stirred for half an hour under nitrogen atmosphere. The colourless solution slowly changed into a yellowish brown indicating the formation of silver nanoparticles. By varying the added percentage of PVP, different sized AgNPs were prepared. After preparing, the AgNPs solution was kept in a sample tube for further use.

6.2.2. Construction of AgNPs-penicillamine-Au electrode modified gold electrode

A gold electrode was polished with wet α-alumina (0.5 μm) on a flat polishing pad for 10 minutes and rinsed several times with doubly distilled water. The cleanliness of the gold electrode surface was ascertained by recording the repetitive cyclic voltammograms in 0.5 M H_2SO_4 between - 0.2 and + 1.5 V *versus* Ag/AgCl with 0.1 V/s scan rate until a steady characteristic gold oxide cyclic voltammogram was obtained.[17] The electrode was then rinsed with doubly distilled water and immersed in 1.0 mM ethanolic solution of penicillamine (PCA) for 24 hours. The PCA was self-assembled over the gold electrode surface *via* gold-sulphur interaction and the modified electrode PCA-Au was thoroughly washed with double distilled water. Thereafter, the PCA modified gold electrode was dipped into AgNPs solution for 4 hours under stirring condition and AgNPs-PCA modified gold electrode (AgNPs-PCA-Au) was formed. The finally modified electrode was washed thoroughly with distilled water and dried in air for further use.

6.3. Results and Discussion

6.3.1. Characterization of AgNPs

6.3.1.1. HR-TEM

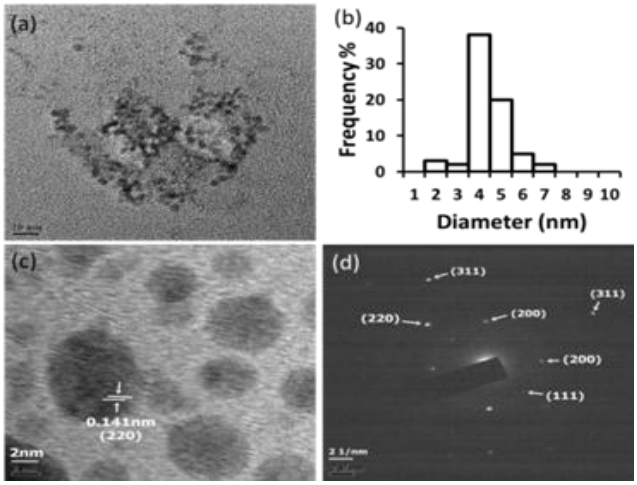

Fig. 6.1. TEM images of AgNPs (scale bar 20 nm) (a), Particle size distribution histogram of AgNPS (b), HRTEM image showing lattice fringes (c), and a typical SAED of AgNPs (d).

To investigate morphological features of the prepared AgNPs, TEM image was recorded and is shown in Fig. 6.1a. The corresponding particle size distribution histogram is given in Fig. 6.1b which shows that the diameter of the nanoparticles is around 4 nm. Fig. 6.1c shows the lattice fringes (0.141nm) on the surface, which is in good agreement with the inter-planer spacing of Ag (220). The nanocrystalline nature of AgNPs was evidenced by the selected area electron diffraction (SAED) pattern. Fig. 6.1d with bright circular spots corresponding to (111), (200), (220) and (311) characteristic of the face centred cubic Ag (JCPDS card no. 89-3722).

6.3.1.2. UV-vis spectroscopy

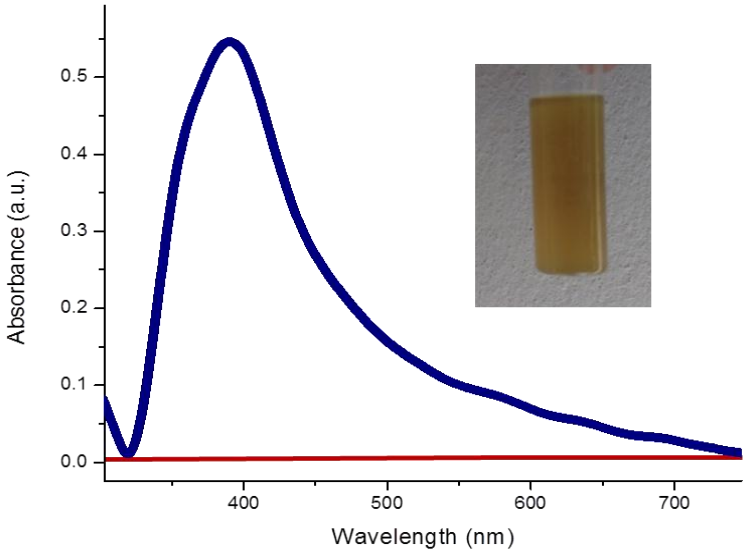

Fig. 6.2. UV-Vis spectra of PVP stabilized AgNPs. [Blue line: $AgNO_3$+ PVP + Ascorbic acid + EtOH; Red line: $AgNO_3$+ PVP + EtOH]

UV-visible spectra of AgNPs@PVP in ethanol (Fig. 6.2) shows a single and sharp surface resonance resonance peak at 390 nm [18] and support the formation of nearly spherical silver nanoparticles.

6.3.2. Characterization of modified electrode

6.3.2.1. FE-SEM and elemental mapping

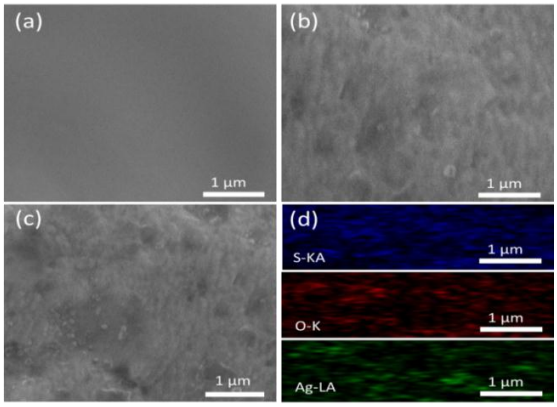

Fig. 6.3. FE-SEM images of bare (a), PCA modified (b) AgNPs-PCA modified gold electrode (c) and elemental mapping of AgNPs-PCA modified gold electrode (d).

The stepwise modification of pure gold electrode surface was characterized by FE-SEM (Fig. 6.3). Fig. 6.3a shows a smooth surface morphology for bare gold electrode and remains almost smooth after modification with PCA (Fig. 6.3b) suggesting well-ordered and densely packed layer formation over gold surface. After immobilization of AgNPs over the PCA-Au, no characteristic change of the surface morphology was observed (Fig. 6.3c) and this may be due to very small particle size (4 nm) of AgNPs. Elemental mapping images show the presence of O, S and Ag which confirms the formation of AgNPs-PCA-Au electrode (Fig. 6.3d).

6.3.2.2. Electrochemical characterization

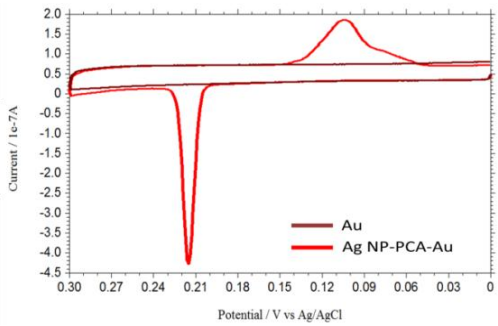

Fig. 6.4. Cyclic voltammograms obtained at bare and AgNPs-PCA modified gold electrode in 0.1 M PBS (pH 7.0).

The electrochemical behaviour of AgNPs was studied using cyclic voltammetry. Fig. 6.4 illustrates the cyclic voltammograms obtained at bare, and AgNPs-PCA modified gold electrode in 0.1 M PBS (pH 7.0). A sharp irreversible oxidation peak was observed at + 0.215 V *versus* Ag/AgCl at AgNPs-PCP-Au electrode whereas no such characteristic peak was observed for bare-Au electrode in the same potential region. This observation reveals that the AgNPs over PCA-Au electrode are more prone to oxidation as compared to reduction, which can be attributed to the reaction $Ag^{\circ} \rightarrow Ag^{+} + e^{-}$.

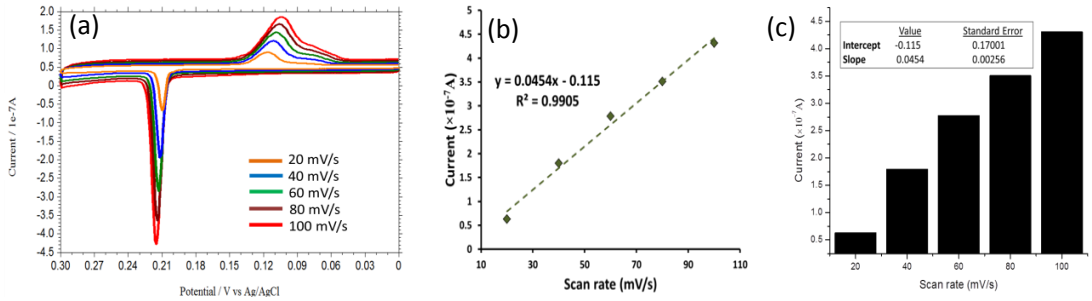

Fig. 6.5. Overlaid cyclic voltammograms obtained with increasing scan rate at AgNPs-PCA-Au electrode in 0.1 M PBS (pH 7.0) (a). Plot of current as a function of scan rate with a linear trend line ($R^2 > 0.99$) (b), Bar diagram of current *versus* scan rate (c).

Fig. 6.5a shows that with increasing scan rate, the oxidation peak of AgNPs was enhanced and at the same time the peak potential was slightly shifted positively with increasing scan rate. The linear variation of peak current with scan rate (Fig. 6.5b) indicates surface confined process involved in the electrode reaction due to the formation of thin layer of AgNPs over PCA-Ag. The characterization of AgNPs-PCA-Au electrode was conducted using the reversible redox couple $[Fe(CN)_6]^{3-}$ / $[Fe(CN)_6]^{4-}$. Fig. 6.6a shows the overlapped cyclic voltammograms of 0.5 mM $[Fe(CN)_6]^{4-}$ in 0.1 M phosphate buffer solution (pH = 7.0) at bare Au, PCA-Au and AgNPs-PCA-Au electrode. A quasireversible redox couple was observed at bare gold electrode and after modification with PCA the oxidation peak was shifted in the positive potential region with decreased in current height which supports the formation of self-assembled monolayer of PCA over Au electrode.

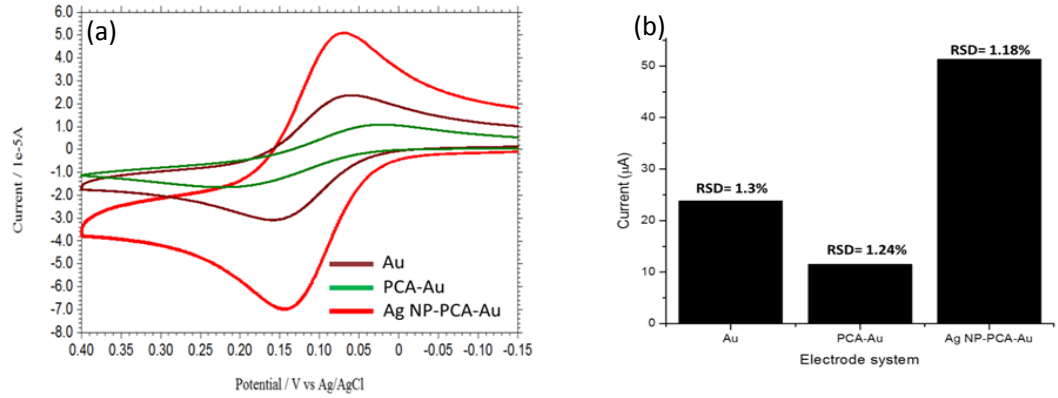

Fig. 6.6. Cyclic voltammograms of 0.5 mM $K_4[Fe(CN)_6]$ in 0.1 M PBS at pH 7.0 using different working electrode (bare Au, PCA-Au and AgNPs-PCA-Au electrode) (a). Bar diagram of cathodic peak current at different electrode system, (b) Five times measurement (n = 5) were taken.

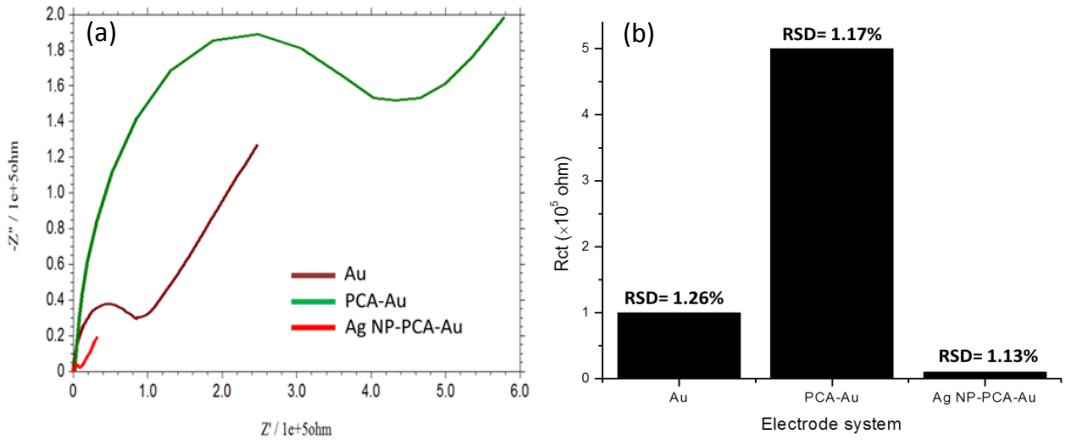

Fig. 6.7. Nyquist plot ($-Z^{//}$ *versus* $Z^{/}$) of 0.5 mM $K_4[Fe(CN)_6]$ in 0.1 M PBS at pH 7.0 using different working electrode (bare Au, PCA-Au and AgNPs-PCA-Au electrode) (a). Bar diagram of R_{ct} values at different electrode system, (b) Five times measurement (n = 5) were taken.

After AgNPs immobilization over PCA-Au electrode, a quasireversible $[Fe(CN)_6]^{4-}$/ $[Fe(CN)_6]^{3-}$ couple (ΔE = 70 mV) was obtained with large increase of peak current height. This is due to the better electronic communication between the redox probe and the gold electrode through AgNPs. Electrochemical impedance spectroscopy (EIS) supports the CV results. In the Nyquist plot (Fig. 6.7a), the

diameter of the semi-circle (R_{ct}) was increased from 1.0×10^5 (bare Au) to 5.0×10^5 Ω (PCA-Au) indicates that the PCA modified Au electrode was blocked the electron transfer between gold electrode and redox probe. After immobilizing AgNPs on the PCA-Au electrode, the R_{ct} values decrease to 0.1×10^5 Ω suggesting low resistance and hence much more electron transfer between the probe and gold electrode through AgNPs. The results also support the proper modification of gold electrode.

6.3.2.3. Electrochemical studies of dopamine and epinephrine at AgNPs-PCA-Au electrode

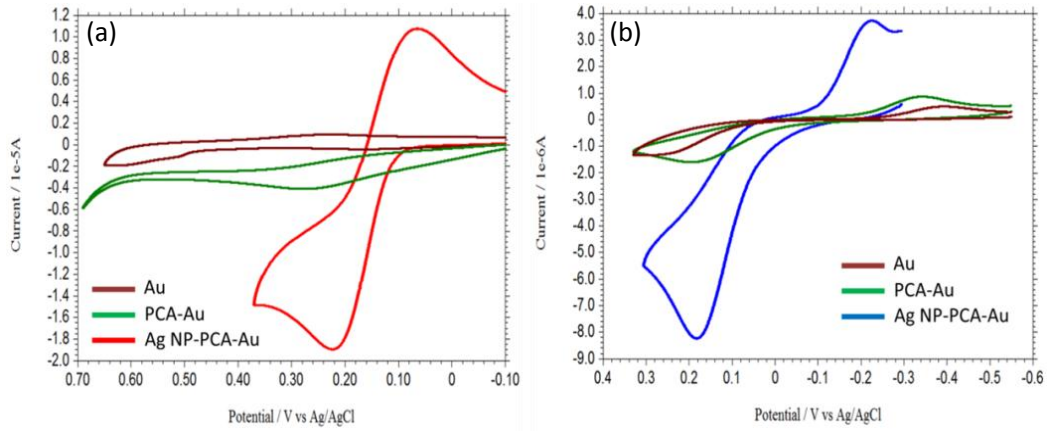

Fig. 6.8. Cyclic voltammogram of 10 μM DA (a) and 10 μM EP (b) in 0.1 M PBS (pH 7.0) at bare, PCA and AgNPs-PCA modified gold electrodes.

Electrocatalytic oxidation of DA and EP were studied using cyclic voltammetry and electrochemical impedance spectroscopy. Cyclic voltammogram of 10 μM DA was recorded in 0.1 M PBS at the bare Au, PCA-Au and AgNPs-PCA-Au with a scan rate of 100 mV/s (Fig. 6.8a). An irreversible redox couple ($\Delta E = E_{pa}-E_{pc} = 0.28$ V) with the anodic peak potential (E_{pa}) at + 0.50 V is observed at the bare gold electrode. At PCA modified gold electrode, the E_{pa} value is shifted to + 0.25 V with increase of current height (I_{pa} = 2.0 μA). Using AgNPs-PCA-Au electrode, a distinct redox couple for DA is observed with large increase of current height (I_{pa} = 15.0 μA) and more negative shifting of the anodic peak potential (+ 0.22 V). Similarly, for EP

the oxidation peak potential is shifted to the less positive potential with large increase of current height when bare, PCA modified and AgNPs-PCA modified gold electrodes is used successively (Fig. 6.8b). These observations support the electrocatalytic nature of AgNPs-PCA-Au electrode for the oxidation of DA and EP. In the EIS experiment, the diameter of the semicircle obtained from the Nyquist plot ($-Z^{//}$ *versus* $Z^{/}$) correspond to the charge transfer resistance (R_{ct}); the smaller the diameter of semicircle, faster is the charge transfer and *vice-versa* .[19] Fig. 6.9 and 6.10 shows that the diameter of the semi-circle decreases upon modification of gold electrode surface.

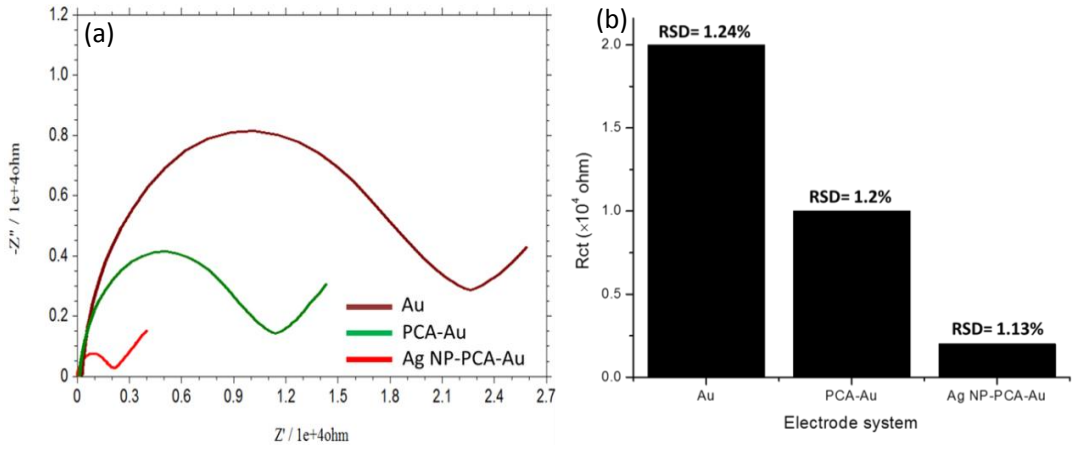

Fig. 6.9. Nyquist plot of 10 µM DA in 0.1 M PBS at pH 7.0 using bare Au, PCA-Au and AgNPs-PCA-Au electrode (a). Bar diagram of R_{ct} values at different *e*lectrode system (b), Five times measurement (n = 5) were taken.

The R_{ct} values in different electrode system shows the following trend: bare Au (2.0×10^4 Ω) > PCA-Au (1.0×10^4 Ω) > AgNPs-PCA-Au (0.2×10^4 Ω) and bare Au (5.0×10^4 Ω) > PCA-Au (3.0×10^4 Ω) > AgNPs-PCA-Au (0.8×10^4 Ω) for DA and EP, respectively. The observed trend suggests that the maximum electron transfer between gold surface and the analyte DA or EP is occurred at AgNPs-PCA-Au electrode. This study also indicates that the AgNPs modified PCA-Au electrode is an efficient electrocatalyst for the oxidation of DA and EP under neutral pH.

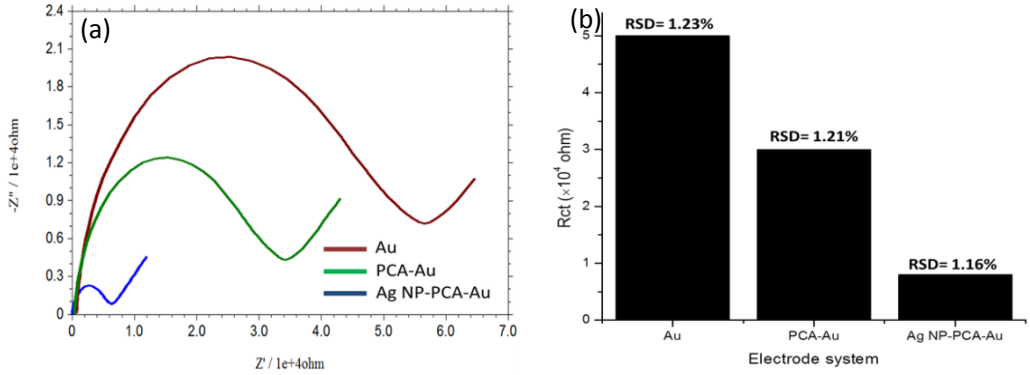

Fig. 6.10. Nyquist plot of 10 µM EP in 0.1 M PBS at pH 7.0 using bare Au, PCA-Au and AgNPs-PCA-Au electrode (a). Bar diagram of R_{ct} values at different *e*lectrode system (b), Five times measurement (n = 5) were taken.

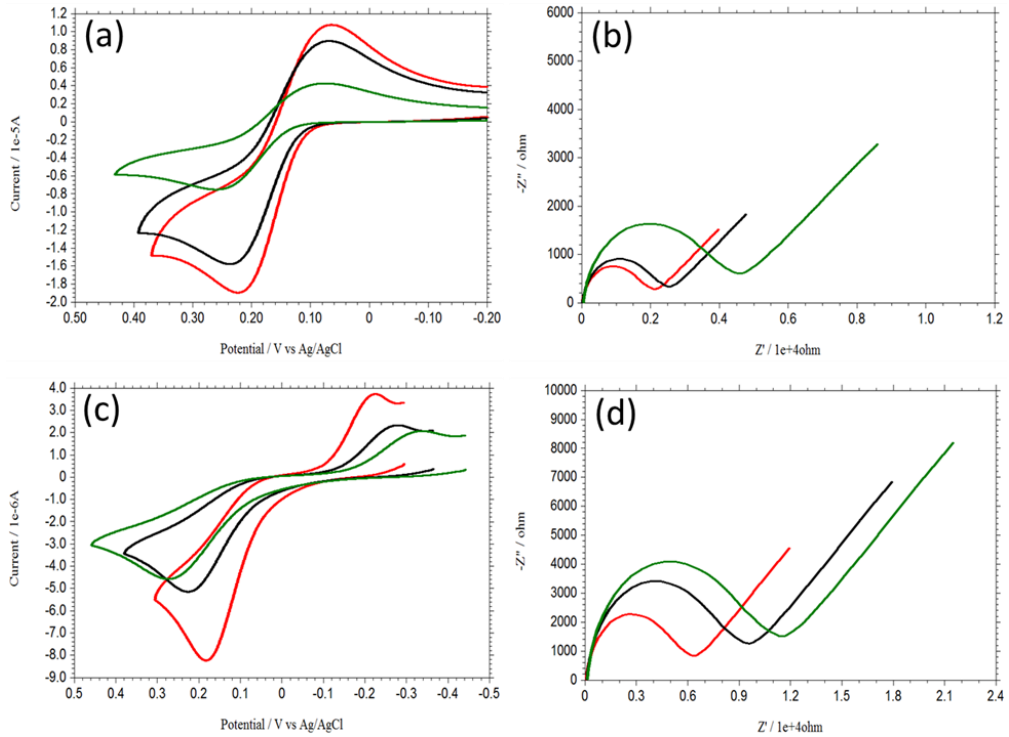

Fig. 6.11. Cyclic voltammogram of 10 µM DA (a) and 10 µM EP (c) in 0.1 M PBS (pH 7.0) at AgNPs (4 nm)-PCA (red curve), AgNPs (10 nm) -PCA (black curve) and AgNPs (20 nm) -PCA (green curve) modified gold electrodes.

To study the size dependent electrochemical sensing behavior of the AgNPs for DA and EP, three different sizes of AgNPs (*viz*., 4, 10 and 20 nm, by varying the

PVP amount as 0.5, 0.3 and 0.1 %, respectively) were employed. The cyclic voltammogram (Fig. 6.11a and 6.11c) shows that the oxidation of DA and EP occurred at low positive potential with large current height at 4 nm sized AgNPs immobilized PCA-Au electrode compared to the 10 or 20 nm AgNPs modified electrode. From the Nyquist plot of 10 μM DA (Fig. 6.11b) in 0.1 M PBS (pH 7.0) using different sized AgNPs modified gold electrodes (E_{ac} = 10 mV, frequency range: 0.01 – 100000 Hz) [AgNPs (4 nm)-PCA-Au (red curve), $R_{ct} = 0.20 \times 10^4$ Ω; AgNPs (10 nm) –PCA-Au (black curve), $R_{ct} = 0.25 \times 10^4$ Ω; and AgNPs (20 nm) –PCA-Au (green curve), $R_{ct} = 0.45 \times 10^4$ Ω] and the nyquist plot of 10 μM EP (Fig. 6.11d) in 0.1 M PBS (pH 7.0) using different sized AgNPs modified gold electrodes (E_{ac} = 10 mV, frequency range: 0.01 – 100000 Hz) [AgNPs (4 nm)-PCA-Au (red curve), $R_{ct} = 0.6 \times 10^4$ Ω; AgNPs (10 nm) –PCA-Au (black curve), $R_{ct} = 0.9 \times 10^4$ Ω; and AgNPs (20 nm) –PCA-Au (green curve), $R_{ct} = 1.2 \times 10^4$ Ω]

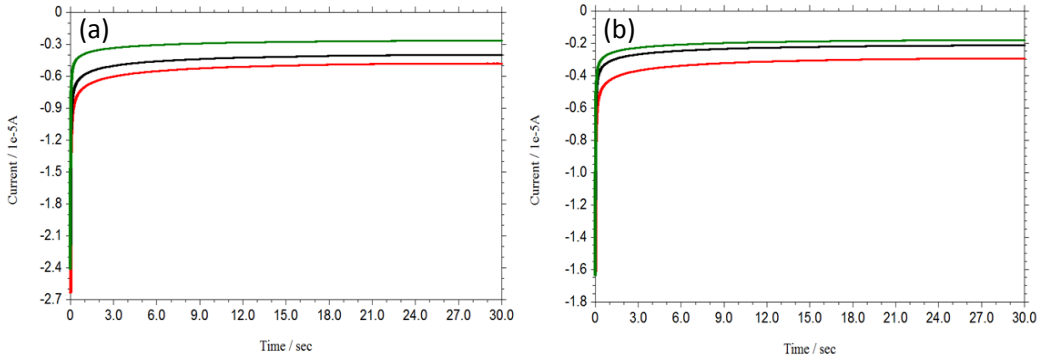

Fig. 6.12. Chronoamperograms of 10 μM DA (a) and 10 μM EP (b) in 0.1 M PBS (pH 7.0) at +0.22 V and +0.18 V *versus* Ag/AgCl, respectively using AgNPs (4 nm)-PCA (red curve), AgNPs (10 nm) -PCA (black curve) and AgNPs (20 nm) -PCA (green curve) modified gold electrodes.

This observation inferred that the 4nm size AgNPs have higher electrocatalytic activity (higher sensing) than the larger size AgNPs. EIS (Fig. 6.11b and 6.11d) and chronoamperometry (Fig. 6.12a and 6.12b) data also supports the higher electrocatalytic sensing ability of AgNPs(4nm)-PCA-Au electrode. By considering

the size dependency results, ~ 4 nm sized AgNPs immobilized PCA-gold electrode is used in the subsequent experiments.

6.3.2.4. Determination of dopamine and epinephrine

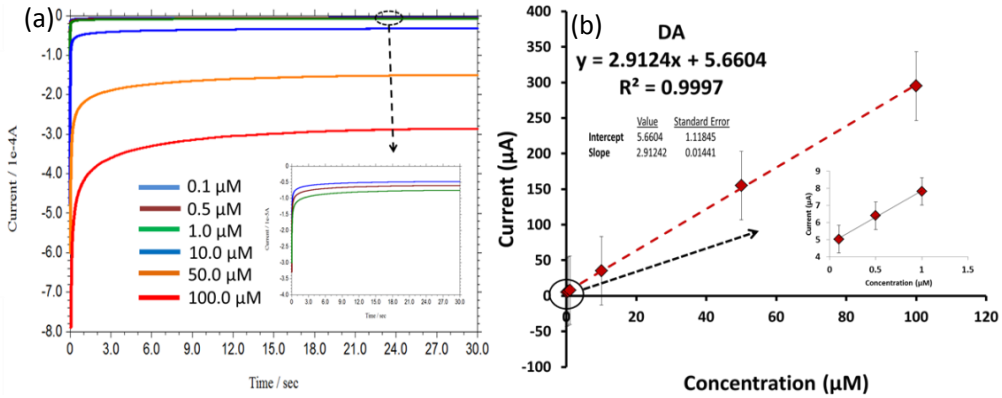

Fig. 6.13. Chronoamperograms with increasing concentration of DA (0.1 to 100.0 mM) in 0.1 M PBS (pH 7.0) using AgNPs-PCA-Au electrode at + 0.22 V *versus* Ag/AgCl, LOD = 0.2 nM (S/N = 3) (a). Plot of resulting current in chronoamperometry at 30 seconds *versus* concentration of DA (b), Five times measurement were taken (n = 5).

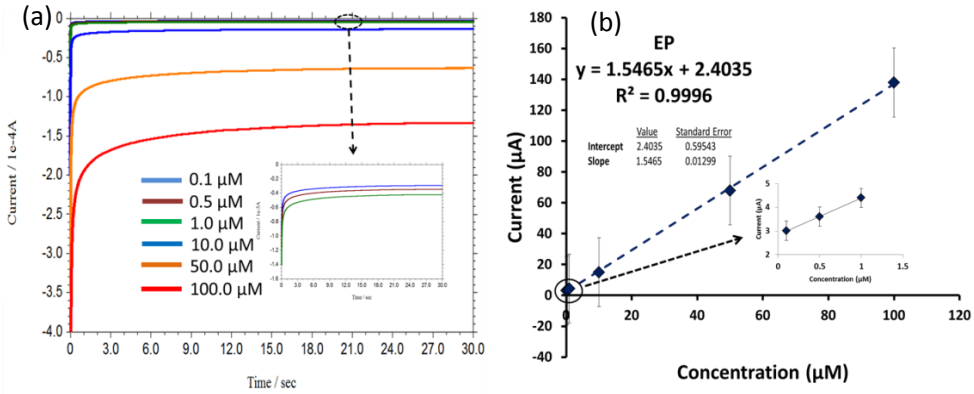

Fig. 6.14. Chronoamperograms with increasing concentration of EP (0.1 to 100.0 mM) in 0.1 M PBS (pH 7.0) using AgNPs-PCA-Au electrode at + 0.18 V *versus* Ag/AgCl, LOD = 0.5 nM (S/N = 3) (a). Plot of resulting current in chronoamperometry at 30 seconds *versus* concentration of EP (b), Five times measurement were taken (n = 5).

Determination of DA and EP were performed under optimized condition using Chronoamperometry. Fig. 6.13 and 6.14 shows the chronoamperograms at the fixed potential + 0.22 V and + 0.18 V (*versus* Ag/AgCl) with increasing concentration of DA and EP in 0.1 M PBS using AgNPs-PCA-Au as working electrode, respectively. The current *versus* concentration plots for DA and EP were linear with their concentration in the range of 0.1 to 100 μM at 30 seconds. The linear regration equation were I = 2.9124 C + 5.6602 (R^2 = 0.9997), with a detection limit of 0.20 nM (S/N = 3) and I = 1.5465 C + 2.4035 (R^2 = 0.9996), with a detection limit of 0.51 nM (S/N = 3) for DA and EP, respectively.

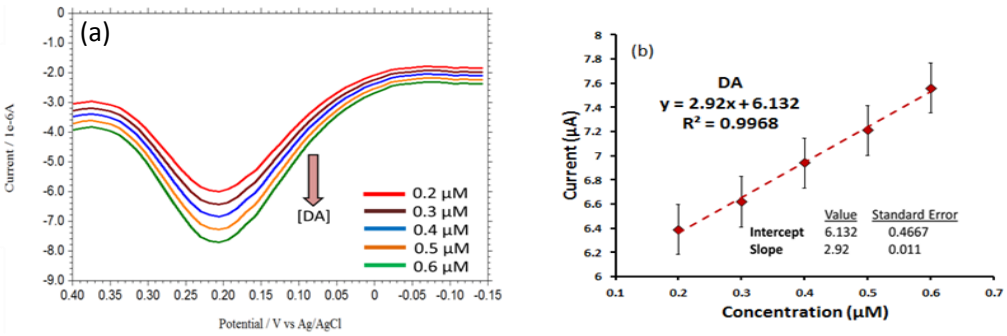

Fig. 6.15. Overlaid DPVs for each increment of 0.1 μM DA at AgNPs-PCA-Au electrode in 0.1 M PBS solution at pH 7.0 (a). A plot of oxidation peak current *versus* increasing concentration of DA (b), Five times measurement were taken(n = 5).

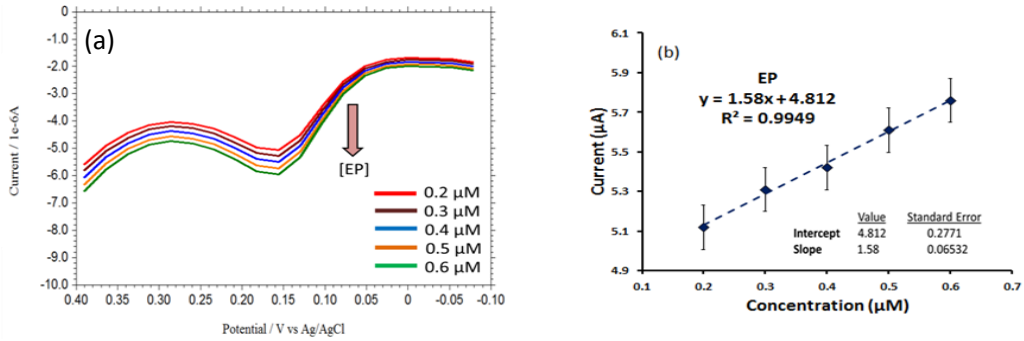

Fig. 6.16. Overlaid DPVs for each increment of 0.1 μM EP at AgNPs-PCA-Au electrode in 0.1 M PBS solution at pH 7.0 (a). A plot of oxidation peak current *versus* increasing concentration of EP (b), Five times measurement were taken(n = 5).

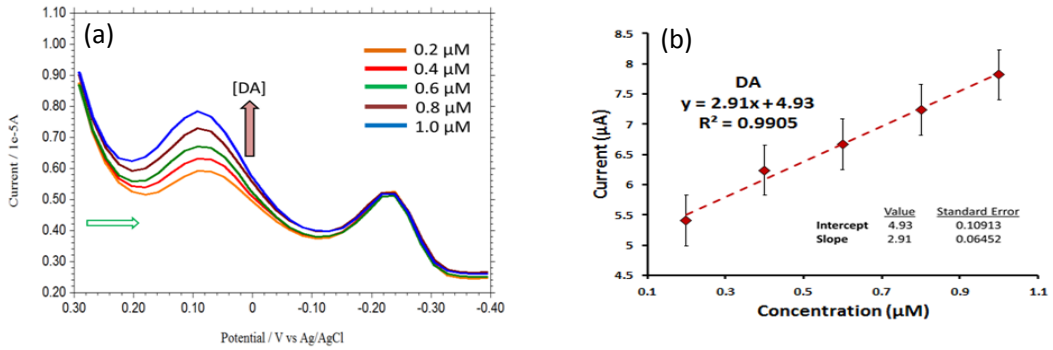

Fig. 6.17. Overlaid differential pulse voltammogram for each increment of 0.2 µM DA to 0.2 µM EP at AgNPs-PCA-Au electrode in 0.1 M PBS buffer solution at pH 7.0 (a). A plot of reduction peak current *versus* increasing concentration of DA (b), Five times measurement were taken(n = 5).

Differential pulse voltammetry was used for further confirmation of the detection limit and the result was satisfactory (Fig. 6.15 and 6.16). Simultaneous determination of DA and EP were performed using DPV. Fig. 6.17 shows the DPV curves of DA with different concentrations in the presence of 0.2 µM EP and the reductive peak current of DA was linear with its concentration range of 0.2 to 1.0 µM. The regression equation was I_{pc} = 2.91 C + 4.93 (R^2 = 0.9905) with a detection limit of 0.20 nM (S/N = 3).

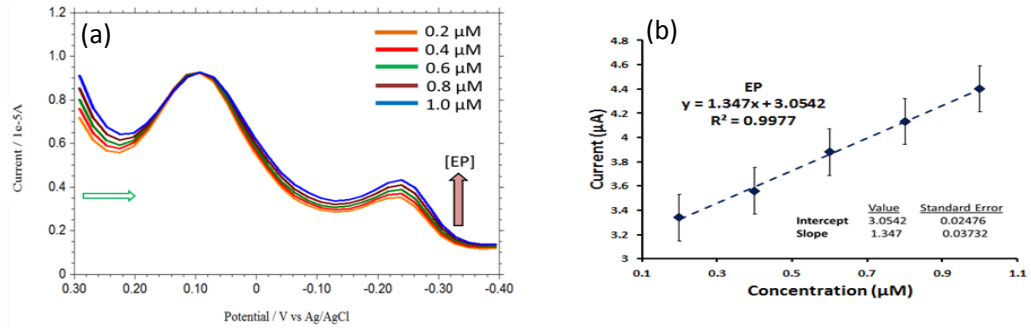

Fig. 6.18. Overlaid differential pulse voltammogram for each increment of 0.2 µM EP to 0.2 µM DA at AgNPs-PCA-Au electrode in 0.1 M PBS buffer solution at pH 7.0 (a). A plot of reduction peak current *versus* increasing concentration of EP (b), Five times measurement were taken(n = 5).

Similarly, Fig. 6.18 shows the DPV curves for different concentration of EP in the presence of fixed concentration (0.2 μM of DA) and the reduction peak current of EP increased linearly in the concentration range of 0.2 to 1.0 μM. The regression equation was I_{pc} = 1.347 C + 3.0542 (R^2 = 0.9977) with a detection limit of 0.51 nM (S/N = 3).

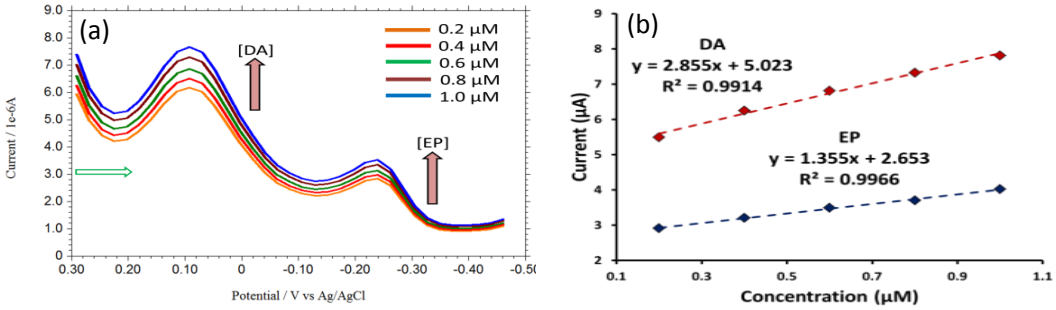

Fig. 6.19. Overlaid DPV for simultaneous increase of concentration of DA and EP in 0.1 M PBS at AgNPs-PCA-Au electrode (a). Plot of current as a function of concentration of DA and EP with linear trend line (b).

For further evaluating the feasibility of the simultaneous determination of DA and EP at AgNPs-PCA-Au electrode, DPV was taken by changing their concentration simultaneously (Fig. 6.19). All the results support the simultaneous and sensitive detection of DA and EP at AgNPs-PCA-Au electrode. Fig. 6.20 shows the DPV of DA and EP in presence of 1000 times higher concentrations of UA and AA and the results support the selective determination of DA and EP is possible in presence of large excess of UA and AA. [Green arrow indicates the scan direction]

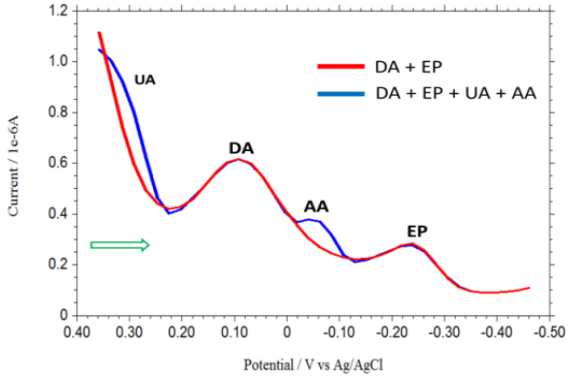

Fig. 6.20. DPVs of 0.2 μM DA and 0.2 μM EP and in presence of 1000 times higher concentration of AA and UA.

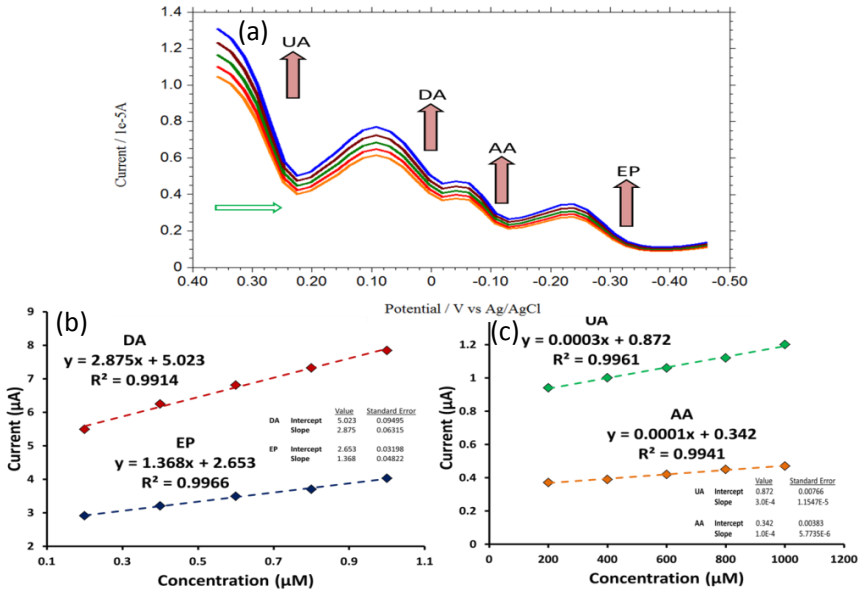

Fig. 6.21. Overlaid differential pulse voltammogram for simultaneous increment of DA, EP, AA and UA at AgNPs-PCA-Au electrode in 0.1 M PBS buffer solution at pH 7.0 (a). Plot of reduction peak current *versus* increasing concentration of DA, EP, AA and UA (b and c), Five times measurement were taken in each case (n = 5).

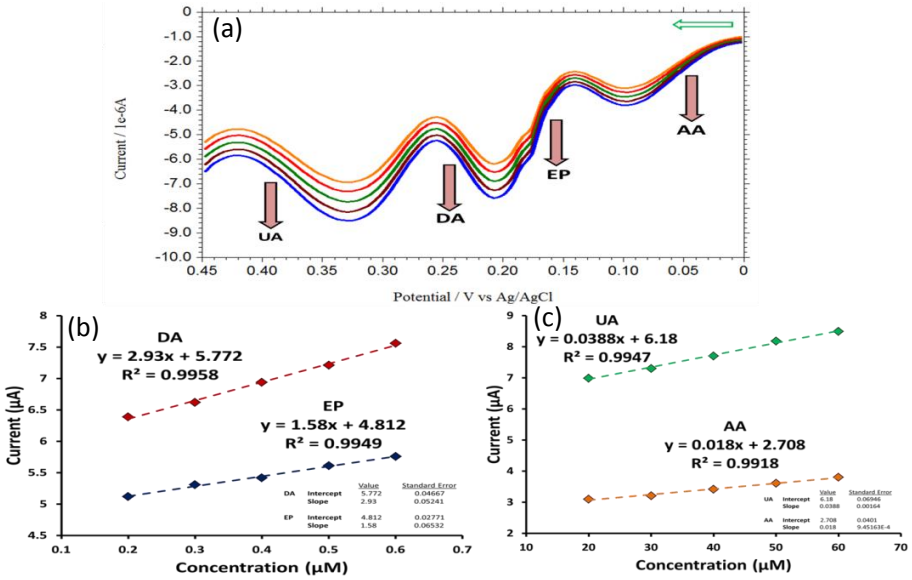

Fig. 6.22. Overlaid DPV for simultaneous increment of DA, EP, AA and UA at AgNPs-PCA-Au electrode in 0.1 M PBS buffer solution at pH 7.0 (a). Plot of oxidation peak current *versus* increasing concentration of DA, EP, AA and UA (b and c), Five times measurement were taken in each case (n = 5).

Fig. 6.21 and 6.22 illustrate the DPV responses of the proposed electrode towards EP, DA, AA and UA when the concentrations of the four species increase simultaneously. It can be seen that both the reduction and oxidation peak current for all four species increases linearly with their concentrations. The DPV responses of the AgNPs-PCA-Au electrode towards the simultaneous determination of these four analytes are listed in Table 6.1.

Table 6.1. Analytical data for the simultaneous determination of EP, DA, UA and AA at AgNPs-PCA-Au electrode.

Species	Linear regression equation	Linear range (μM)	Correlation coefficient (R^2)	Detection limit
DA	I_{pa} = 2.93 C + 5.772	0.2-0.5	0.9958	0.2 nM
EP	I_{pa} = 1.58 C + 4.812		0.9949	0.5 nM
UA	I_{pa} = 0.038 C + 6.180	20-60	0.9947	
AA	I_{pa} = 0.018 C + 2.708		0.9918	
DA	I_{pc} = 2.875 C + 5.023	0.2-1.0	0.9914	0.2 nM
EP	I_{pc} = 1.368 C + 2.653		0.9966	0.5 nM
UA	I_{pc} = 0.0003 C + 0.872	200-1000	0.9961	
AA	I_{pc} = 0.0001 C + 0.342		0.9941	

The RSD of the peak current was less than 2.5 % for these four species at AgNPs modified gold electrode (n = 10). In comparison to other electrochemical sensors, the proposed AgNPs-PCA-Au electrode exhibited improved analytical performance as shown in Table 6.2.

Table 6.2. Comparative account of different electrochemical sensors for DA and EP sensing.

Sensor	DA		EP		Reference
	Linear range (μM)	Detection limit (μM)	Linear range (μM)	Detection limit (μM)	
DNA-Ppyox-CPE	0.3 – 10.0	0.08	0.5– 20	0.06	[1]
α-CD-CNT-GCE	2.0-1000.0	1.0	1.0-1000	0.5	[2]
L-methionine-GCE	1.0 -500.0	0.42	0.5– 100	0.36	[3]
Poly(caffeic)acid-GCE	1.0 – 35.0	0.1	1.0 -35.0	0.2	[4]
PLG-Ag-GCE	5.0-100.0	0.5	10.0-100.0	0.8	[5]
Au/AuO-CMC-Pt	-	0.078	-	0.35	[6]
Polydopamine-nanogold composite-GCE	1.0 – 80.0	0.1	1.0 – 80.0	0.08	[7]
NiONPs-MWCNT-DPH-GCE	0.07– 4.8	0.05	0.37– 9.5	0.082	[8]
AgNPs-SiO_2-GO-GCE	-	0.26	-	0.27	[9]
PCA-Au	20 – 800.0	4.0	-	-	[10]
PCA-Au	-	-	5.0– 200	0.13	[11]
AgNPs-PCA-Au	0.1-100.0	0.0002	0.1-100	0.0005	Present work

Ppyox: overoxidized polypyrrole; α-CD: α-cyclodextrin; PLG-Ag: Silver doped poly(L-glutamic acid); CMC: carboxylated multi-walled carbon nanotubes; GO: graphene oxide; DPH: dihexadecylphosphate; PCA: Penicillamine

6.3.2.5. Effect of scan rate and kinetic analysis for DA and EP oxidation

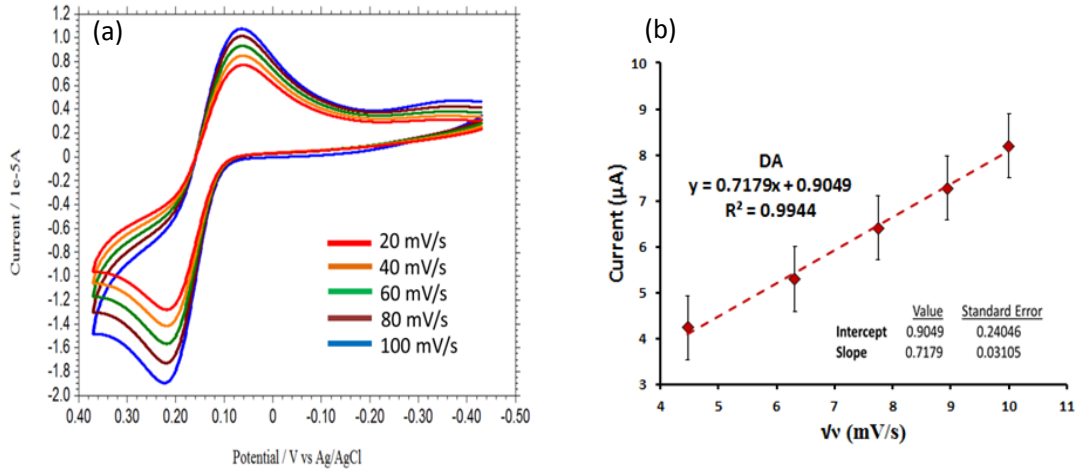

Fig. 6.23. Cyclic voltammograms of 10 µM DA in 0.1 M PBS (pH 7.0) at different scan rate using AgNPs-PCA modified gold electrode (a). Plot of oxidation peak current *versus* square root of scan rate (b), Five times measurement were taken(n = 5).

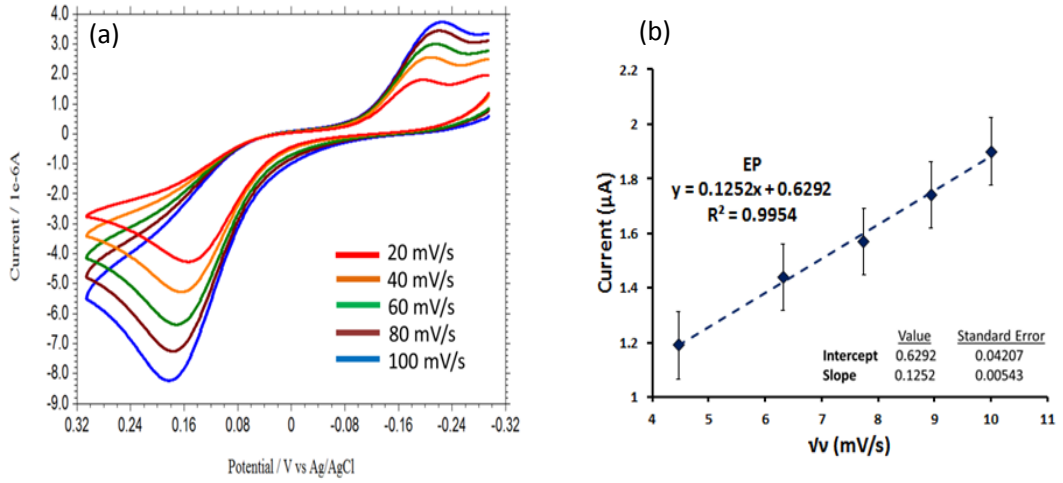

Fig. 6.24. Cyclic voltammograms of 10 µM EP in 0.1 M PBS (pH 7.0) at different scan rate using AgNPs-PCA-Au electrode (a). Plot of oxidation peak current *versus* square root of scan rate (b), Five times measurement were taken(n = 5).

The results showed that with increasing scan rate, the oxidation peak potential (E_{pa}) for DA (Fig. 6.23a) and EP (Fig. 6.24a) are shifted to more positive potential,

confirming the kinetic limitation of the electrochemical reaction.[20] The anodic peak current (I_{pa}) *versus* the square root of the scan rate ($\sqrt{\nu}$) for DA (Fig. 6.23b) and EP (Fig. 6.24b) in the range of 20-100 mV/s was found to be linear following the linear regression equation I_{pa} (μA) = 0.7179 ν (mVs^{-1}) + 0.9049 (R^2 = 0.9944) and I_{pa} (μA) = 0.1251 ν (mVs^{-1}) + 0.6292 (R^2 = 0.9954), respectively. These observations revealed that the electrooxidation reaction of DA and EP was followed pure diffusion controlled electron transfer at AgNPs-PCA-Au electrode.[21] Using the plot (I_{pa} *versus* $\sqrt{\nu}$) and Randles-Sevcik equation $I_{pa} = 2.69 \times 10^5\ n^{3/2}\ A\ D^{1/2}\ C\nu^{1/2}$ …(Eq. 1) [21] the diffusion coefficient (D) was calculated for DA and EP and the values obtained were 13.4×10^{-6} cm^2s^{-1} and 2.1×10^{-6} cm^2s^{-1}, respectively (where I_{pa} is the peak current, n is the number of electron transfer, n = 2 for DA and EP oxidation, A is the electrode area, C is the concentration of electroactive species, and ν is the scan rate at 298 K). The electron transfer coefficient for the quasireversible oxidation of DA and irreversible oxidation of EP at the modified electrode can be determined from the equation $E_p - E_{p/2} = 1.857RT/\alpha F = 47.7/\alpha$ mV……(Eq. 2) [21] where E_p and $E_{p/2}$ represent the peak potential and the half-height peak potential, respectively in cyclic voltammetry experiment where R, F and T have their usual meaning. For DA and EP oxidation, ($E_p - E_{p/2}$) were 46 mV and 48 mV, respectively, hence electron transfer coefficient (α) is calculated to be 0.54 for DA and 0.49 for EP. The standard heterogeneous rate constant (k_s) for the oxidation of DA and EP at AgNPs modified gold electrode was calculated by using the Velasco equation [22] $k_s = 1.11\ D^{1/2}(E_p - E_{p/2})^{-1/2}\nu^{1/2}$ ……(Eq.3). The estimated k_s values for the oxidation of DA and EP at AgNPs-PCA-Au electrodes was found to be 6.1×10^{-3} cm/s and 2.4×10^{-3} cm/s, respectively. The observed higher k_s value for DA and EP at the modified electrode indicates that both the oxidation were faster at the AgNPs-PCA-Au electrode.

6.3.2.6. Effect of solution pH

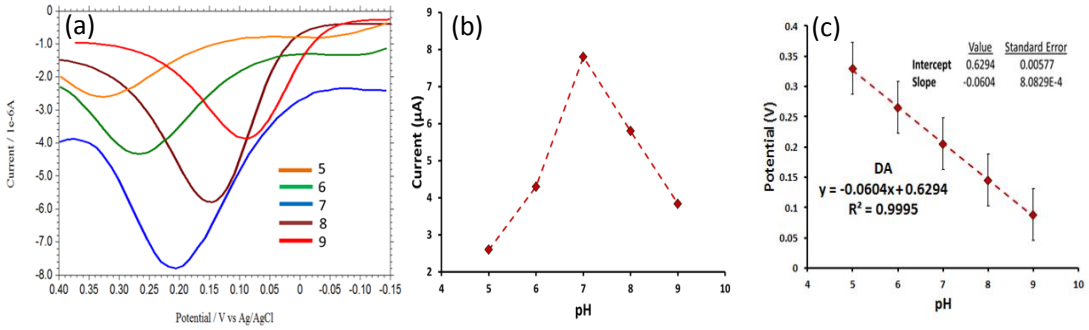

Fig. 6.25. DPVs of 0.6 µM DA in 0.1 M PBS at different pH using AgNPs-PCA modified gold electrode (a), Plot of anodic peak current of 0.6 µM DA *versus* pH(b), Plot of oxidation peak potential of 0.6 µM DA *versus* pH(c), Five times measurement were taken(n = 5).

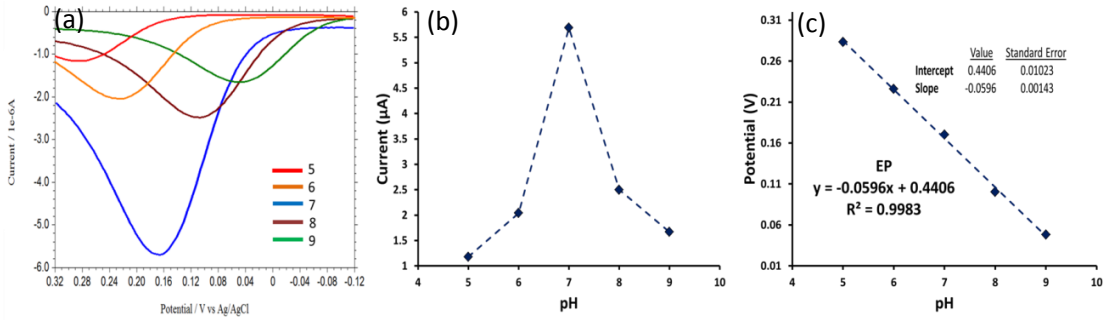

Fig. 6.26. DPVs of 0.6 µM EP in 0.1 M PBS at different pH (5.0 - 9.0) using AgNPs-PCA modified gold electrode (a), Plot of anodic peak current of 0.6 µM EP *versus* pH(b), Plot of oxidation peak potential of 0.6 µM EP *versus* pH(c), Five times measurement were taken(n = 5).

The role of pH on the electrooxidation of DA and EP at AgNPs modified Au electrode were scrutinized in the pH range of 5.0-9.0. (Fig. 6.25a and 6.26a) Exploration of the impact of pH on the peak current of DA and EP at the AgNPs-PCA-Au electrode tells that the peak current was reached maximum for DA and EP at pH 7.0 and thereafter decreased by increasing pH of the solution (Fig. 6.25b and 6.26b). At pH 7.0, DA and EP mostly exists as a protonated form ($^{+}NH_3$-DOH or

$^{+}NH_2$-EOH with D and E for DA and EP skeletons, respectively) [23,24] and therefore readily pre-concentrated on the negatively charged [AgNPs-($^{-}$OOC-C(NH_2)-C(CH_3)$_2$-S)] thin layer modified gold electrode and showing maximum current height. Above pH 7.0, the anodic peak current decreased and this may be due to the repulsion between the anionic form of DA or EP (NH_2-DO^{-} or NH-EO^{-}) and the negatively charged AgNPs-($^{-}$OOC-C(NH_2)-C(CH_3)$_2$-S-Au electrode. By considering the pH dependency results, we have selected pH 7.0 for DA and EP in the subsequent experiments. The anodic peak potential for DA and EP changes linearly with pH between 5-9, and is shifted to more negative potentials following the linear regression equation E_{pa} (V) = - 0.0604 pH + 0.0629 (R^2 = 0.999) and E_{pa} (V) = - 0.0596 pH + 0.4406 (R^2 = 0.998), respectively (Fig. 6.25c and 6.26c). The slope of 60.0 and 59.6 mV/pH suggested that equal number of protons and electrons were participated in the electrode reaction process.[25] The negative shifting of anodic peak potential indicates that the proton liberation from DA and EP is facilitated (less energy required for DA and EP oxidation) with increasing pH of the medium.

6.3.2.7. Reproducibility, sensitivity and stability

Reproducibility and long term stability is highly desirable for the practical applications and commercialization of any electrochemical sensor. The reproducibility of the AgNPs-PCA-Au electrode was examined by 10 repetitive measurements for DA and EP in 0.1 M PBS solution. The results showed that the oxidative peak current for DA and EP remain same with a relative standard deviation (RSD) of 0.04 and 0.03 %, respectively, suggesting that the modified electrode has a good reproducibility. The AgNPs modified gold electrode was highly sensitive towards DA and EP and the sensitivity were 97.33 and 52.3 $\mu Acm^{-2}\mu M^{-1}$, respectively. The long term stability was monitored by taking CV at 5 days intervals for 30 days. After each use the sensor was washed, dried and stored at room temperature by covering with a rubber cap. Up to 30 days monitoring, the sensor retained 100% of its original current response for DA and EP in 0.1 M PBS.

6.3.2.8. Interference study

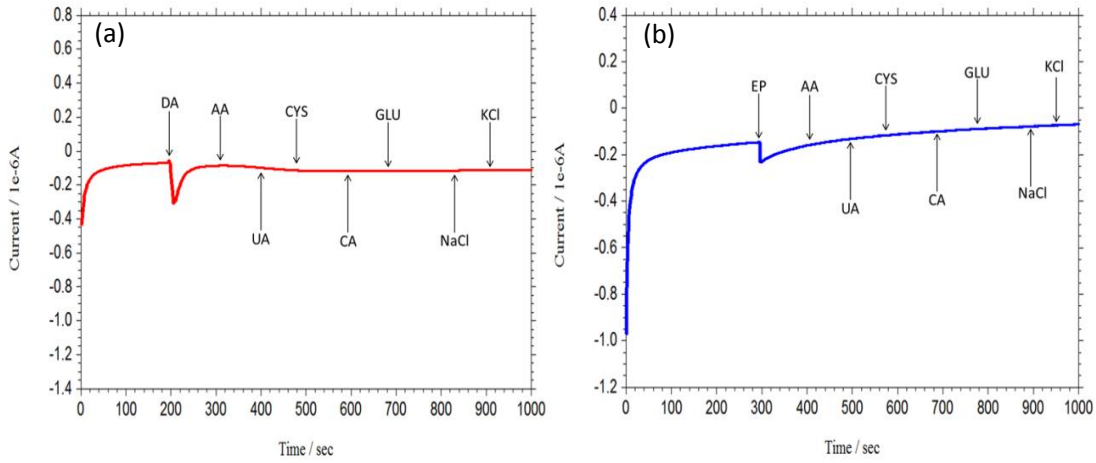

Fig. 6.27. Amperometric response at AgNPs-PCA-Au with an applied potential of + 0.22 V on subsequent addition of 0.01 μM DA, 1.0 μM AA, 1.0 μM UA, 1.0 μM Cys, 1.0 μM CA, 1.0 μM Glu, 1.0 μM NaCl, 1.0 μM KCl under stirring condition (a). Amperometric response at AgNPs-PCA-Au electrode with an applied potential of + 0.18 V on subsequent addition of 0.01 μM EP, 1.0 μM AA, 1.0 μM UA, 1.0 μM Cys, 1.0 μM CA, 1.0 μM Glu, 1.0 μM NaCl, 1.0 μM KCl under stirring condition (b) (Supporting electrolyte: 0.1 M PBS, pH 7.0).

The influence of various interfering agents such as ascorbic acid, uric acid, citric acid, cysteine, glucose and different ions e.g. Na^+, K^+, Cl^- etc on the determination of DA and EP were evaluated under optimum conditions. Fig. 6.27a and 6.27b shows the amperometric response for DA and EP at AgNPs-PCA-Au electrode in the presence of tenfold excess interferents at 0.22 and 0.18 V, respectively in 0.1 M PBS under stirring condition. With the addition of these interfering substances no obvious current response was observed, however, with the addition of DA and EP the sharp current response were appeared. These results suggest that the sensor is highly selective for DA and EP detection.

6.3.2.9. Real sample analysis

To evaluate the feasibility of proposed AgNPs-PCA-Au sensor for the determination of DA and EP in real sample, human blood was taken. Standard addition method was used to determine the ability of the proposed electrochemical sensor. Fig. 6.28a shows the DPV of blood sample solution (1.0 mL blood samples diluted with 4 mL 0.1 M in PBS, pH 7.0) and after addition of standard DA and EP solution in blood sample solution. The DPV of blood sample shows the reduction of DA and EP at 0.09 V and 0.23 V, respectively. The content of DA and EP in blood sample was calculated 0.42 μM (0.0064 mg/dL) and 0.21 μM (0.0039 mg/dL), respectively using the standard addition method and the direct interpolation of the linear regression (RSD = 1.14 % and RSD = 1.21 % for DA and EP, respectively). The accuracy of the method was also verified by recovery study by adding standard DA and EP solution to the real sample and around 99-100.5 % recoveries were obtained. The same sensor can able to detect AA and UA in blood sample (Fig. 6.28b). The results are summarized in Table 6.3. The results indicate that the modified electrode can effectively detect DA, EP, UA and AA in human blood sample.

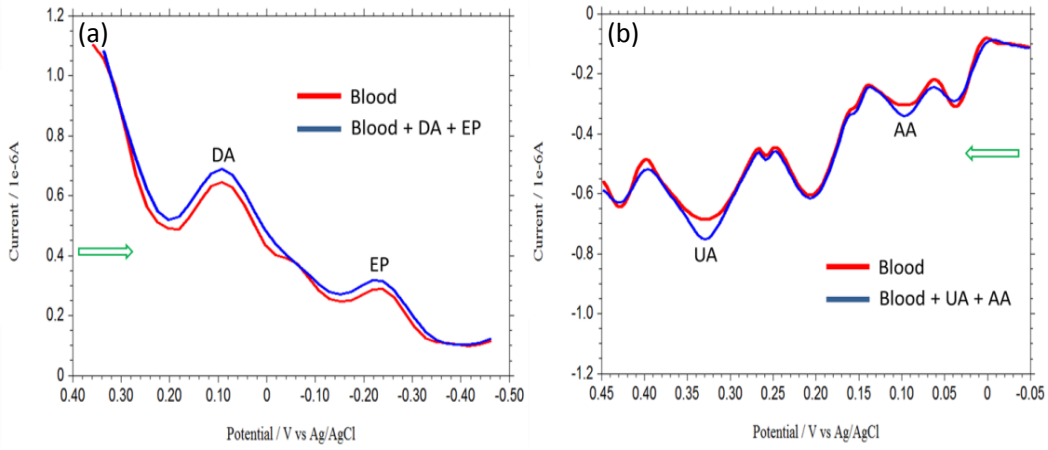

Fig. 6.28. Overlaid DPV of human blood sample solution and after addition of standard DA and EP (a). Overlaid DPVs of human blood sample solution and after addition of standard UA and AA solution in blood sample solution (b). [Green arrow shows scan direction]

Table 6.3. Determination of DA, EP, AA and UA in blood sample.

Analyte in blood	Detected (μM)	Spiked (μM)	Found (μM)	RSD[a] (%)	Recovery (%)
DA	0.42	0.2	0.201	1.14	100.5
EP	0.21	0.2	0.198	1.21	99.0
AA	62.14	10.0	10.030	2.37	100.3
UA	36.27	15.0	15.240	1.53	101.6

[a] Five times measurement were taken.

6.4. Conclusions

In this work, a new electrochemical sensor AgNPs-Penicillamine-Au was introduced for the simultaneous determination of DA and EP in presence of AA and UA. DPV shows all four distinct reduction peaks for DA, EP, AA and UA. The sensor showed high sensitivity, excellent selectivity, and long linear dynamic range with low detection limit of as low as nanomolar range. Furthermore, the sensor has higher potential for real sample application and was proved by the simultaneous determination of DA, EP and AA, UA in human blood sample.

6.5. References

1. D. J. Michael and R. M. Wightman, *J. Pharm. Biomed. Anal.*, 1999, **19**, 33; R. M. Wightman, L. J. May and A. C. Michael, *Anal. Chem.*, 1988, **60**, 769A.
2. J.W. Zheng, Y. Yang, S. H. Tian, J. Chen, F. A. W. Wilson and Y. Y. Ma, *Neurosci. Lett.*, 2005, **382**, 164; N. Nakao, T. Itakura, *Progress in Neurobiology*, 2000, **61**, 313.
3. T. N. Deftereos, A. C. Calokerinos and C. E. Efstathiou, *Analyst*, 1993, **118**, 627; M. H. Sorouraddin, J. L. Manzoori, E. Kargarzadeh and A. M. Haji Shabani, *J. Pharm. Biomed. Anal*., 1998, **18**, 877.
4. V. Carrera, E. Sabater, E. Vilanova and M. A. Sogorb, J. Chromatogr, B: Anal. Technol. *Biomed. Life Sci*., 2007, **847**, 88.
5. J. Z. Kang, X. B. Yin, X. R. Yang and E. K. Wang, *Electrophoresis*, 2005, **26**, 1732.
6. Y. Su, J. Wang and G. N. Chen, *Talanta*, 2005, **65**, 531.
7. N. T. Deftereos, A. C. Calokerinos and C. E. Efstlectrochathiou, *Analyst*, 1993, **118**, 627; J. X. Du, L. H. Shen and J. R. Lu, *Anal. Chim. Acta*, 2003, **489**, 183-189.
8. M. Zhu, X. Huang, J. Li and S. Hansi, *Anal. Chim. Acta*, 1997, **357**, 261.
9. Y. Wang and Z. –Z. Chen, *Colloids Surf. B*, 2009, **74**, 322.
10. Y. Zhang, W. Ren and S. Zhang, *Int. J. Electrochem. Sci*., 2013, **8**, 6839.
11. A. Ulman, *Chem. Rev*., 1996, **96**, 1533.
12. Q. Wang, D. Dong and N. Li, *Bioelectrochemistry*, 2001, **54**, 169.
13. L. M. Niu, H. Q. Luo and N. B. Li, *Microchim. Acta*, 2005, **150**, 87-93.
14. Y. G. Sun and Y. N. Xia, *Science*, 2002, **298**, 2176.
15. T. Sun and K. Seff, *Chem. Rev*., 1994, **94**, 857.
16. F. J. Smally, K. Chalfant, S. W. Feldberg, T. M. Nahir and E. F. Bowden, *J. Phys. Chem. B*, 1999, **103**, 1676.
17. R. K. Shervedani, A. Hatefi-Mehrjardi and M. Khosravi Babadi, *Electrochim. Acta*, 2007, **52**, 7051.

18. T. A. Afify, H. H. Saleh and Z. I, Ali, *Polym. Compos.*, 2015, DOI 10.1002/pc23866., B. Ajitha, Y. A. K. Reddy and P. S. Reddy, *Powder Technol*., 2015, **269**,110.
19. P. N. Mashazi, P. Westbroek, K. I. Ozoemena and T. Nyokong, *Electrochim. Acta*, 2007, **53**, 1858.
20. C. S. Shen, Y. Z. Wen, Z. L. Shen, J. Wu and W. P. Liu, *J. Hazard. Mater*., 2011, **193**, 209.
21. A. J. Bard and L. R. Faulkner, *Electrochemical Methods Fundamental and Applications*, John Wiley & Sons Inc., New York, 2001.
22. J. G. Velasco, Electroanalysis, 1997, **9**, 880.
23. J. L. Berfield, L. C. Wang and M. E. A. Reith, *J. biol. Chem*., 1999, **274**, 4876.
24. R. C. Reynolds and H. F. Hardman, *Eur. J. pharmacol*., 1972, **20**, 249.
25. E. Laviron, *J. Electroanal. Chem*., 1974, **52**, 355.